

# SANDIA REPORT

SAND2014-1546

Unlimited Release

Printed February 2014

## Experimental Comparison of PV-Smoothing Controllers using Distributed Generators

Jay Johnson, Kimio Morino, Atsushi Denda, John Hawkins, Brian Arellano, Takao Ogata, Takao Shinji, Masayuki Tadokoro, and Abraham Ellis

Prepared by  
Sandia National Laboratories  
Albuquerque, New Mexico 87185 and Livermore, California 94550

Sandia National Laboratories is a multi-program laboratory managed and operated by Sandia Corporation, a wholly owned subsidiary of Lockheed Martin Corporation, for the U.S. Department of Energy's National Nuclear Security Administration under contract DE-AC04-94AL85000.

Approved for public release; further dissemination unlimited.



**Sandia National Laboratories**

Issued by Sandia National Laboratories, operated for the United States Department of Energy by Sandia Corporation.

**NOTICE:** This report was prepared as an account of work sponsored by an agency of the United States Government. Neither the United States Government, nor any agency thereof, nor any of their employees, nor any of their contractors, subcontractors, or their employees, make any warranty, express or implied, or assume any legal liability or responsibility for the accuracy, completeness, or usefulness of any information, apparatus, product, or process disclosed, or represent that its use would not infringe privately owned rights. Reference herein to any specific commercial product, process, or service by trade name, trademark, manufacturer, or otherwise, does not necessarily constitute or imply its endorsement, recommendation, or favoring by the United States Government, any agency thereof, or any of their contractors or subcontractors. The views and opinions expressed herein do not necessarily state or reflect those of the United States Government, any agency thereof, or any of their contractors.

Printed in the United States of America. This report has been reproduced directly from the best available copy.

Available to DOE and DOE contractors from

U.S. Department of Energy  
Office of Scientific and Technical Information  
P.O. Box 62  
Oak Ridge, TN 37831

Telephone: (865) 576-8401  
Facsimile: (865) 576-5728  
E-Mail: [reports@adonis.osti.gov](mailto:reports@adonis.osti.gov)  
Online ordering: <http://www.osti.gov/bridge>

Available to the public from

U.S. Department of Commerce  
National Technical Information Service  
5285 Port Royal Rd.  
Springfield, VA 22161

Telephone: (800) 553-6847  
Facsimile: (703) 605-6900  
E-Mail: [orders@ntis.fedworld.gov](mailto:orders@ntis.fedworld.gov)  
Online order: <http://www.ntis.gov/help/ordermethods.asp?loc=7-4-0#online>



# Experimental Comparison of PV-Smoothing Controllers using Distributed Generators

Jay Johnson and Abraham Ellis  
Sandia National Laboratories  
P.O. Box 5800  
Albuquerque, New Mexico 87185-0352

Atsushi Denda and Kimio Morino  
Shimizu Corporation

John Hawkins and Brian Arellano  
Public Service Company of New Mexico

Takao Shinji, Takao Ogata, and Masayuki Tadokoro  
Tokyo Gas Co., Ltd.

## Abstract

The power output variability of photovoltaic systems can affect local electrical grids in locations with high renewable energy penetrations or weak distribution or transmission systems. In those rare cases, quick controllable generators (e.g., energy storage systems) or loads can counteract the destabilizing effects by compensating for the power fluctuations. Previously, control algorithms for coordinated and uncoordinated operation of a small natural gas engine-generator (genset) and a battery for smoothing PV plant output were optimized using MATLAB/Simulink simulations. The simulations demonstrated that a traditional generation resource such as a natural gas genset in combination with a battery would smooth the photovoltaic output while using a smaller battery state of charge (SOC) range and extending the life of the battery. This paper reports on the experimental implementation of the coordinated and uncoordinated controllers to verify the simulations and determine the differences in the controllers. The experiments were performed with the PNM PV and energy storage Prosperity site and a gas engine-generator located at the Aperture Center at Mesa Del Sol in Albuquerque, New Mexico. Two field demonstrations were performed to compare the different PV smoothing control algorithms: (1) implementing the coordinated and uncoordinated controls while switching off a subsection of the PV array at precise times on successive clear days, and (2) comparing the results of the battery and genset outputs for the coordinated control on a high variability day with simulations of the coordinated and uncoordinated controls. It was found that for certain PV power profiles the SOC range of the battery may be larger with the coordinated control, but the total amp-hours through the battery—which approximates battery wear—will always be smaller with the coordinated control.

## **ACKNOWLEDGMENTS**

This work was funded by the U.S. Department of Energy Solar Energy Technologies Program and Office of Electricity Energy Storage Program. We also acknowledge the contribution of Public Service Company of New Mexico (PNM), as well as Japan's New Energy and Industrial Development Organization (NEDO), Shimizu and Tokyo Gas for executing the demonstrations.

# CONTENTS

<b>CONTENTS .....</b>	<b>5</b>
<b>FIGURES .....</b>	<b>6</b>
<b>TABLES.....</b>	<b>6</b>
<b>NOMENCLATURE.....</b>	<b>7</b>
<b>1. INTRODUCTION.....</b>	<b>9</b>
<b>2. SMOOTHING ALGORITHMS .....</b>	<b>11</b>
2.1 Battery Energy Storage System (BESS).....	11
2.2 Building Energy Management System (BEMS).....	12
2.3 Combined Gas Genset (BEMS) and Battery (BESS) Controllers .....	15
<b>3. COMMUNICATIONS.....</b>	<b>17</b>
3.1 Operational Historian Configuration Settings .....	19
3.2 Communications Latencies .....	21
3.3 Communication Dropouts.....	22
<b>4. EXPERIMENTAL DEMONSTRATIONS .....</b>	<b>23</b>
4.1 Experimental Setup.....	24
4.2 Real-time Demonstration of Coordinated and Uncoordinated Control with Artificial PV Variability .....	25
4.3 Comparison of real-time coordinated control to simulated controllers .....	29
<b>5. CONCLUSIONS.....</b>	<b>35</b>
<b>REFERENCES.....</b>	<b>36</b>
<b>DISTRIBUTION.....</b>	<b>38</b>

## FIGURES

Figure 1: PNM Prosperity BESS controller [2, 3].	12
Figure 2: MdS BEMS controller with genset and fuel cell.	13
Figure 3: MdS BEMS controller with only a genset.	14
Figure 4: Comparison of low-pass and band-pass filters. The output power from the GE will be the same when selecting $T_1 = T_{High} = 160$ sec, and $T_{Low} < 20$ sec.	14
Figure 5: The GE setpoint and active output power when a 90 kW step increase in the PV power is observed.	15
Figure 6: Control schemes for the battery and gas engine-generator.	16
Figure 7: Geographical locations of the PNM Prosperity Site and Mesa del Sol Aperture Center.	17
Figure 8: Control schemes for the battery/FC and gas engine-generator for Test A.	19
Figure 9: Data compression and exemption rules at the MdS PI server caused the step changes in the BEMS $P_{PV}$ profile.	21
Figure 10: Communication latency in the PI-PI link.	21
Figure 11: $P_{PV}$ communication errors between the MdS PI server and BEMS. The dropouts occur when $P_{PV} = 0$ .	22
Figure 12: Gas engine setpoint and output power changes due to $P_{PV}$ data dropouts.	22
Figure 13: Test procedure for the real-time PV output step change.	25
Figure 14: PV power variability between tests days.	26
Figure 15: Simulation and experimental results for battery and gas engine output power for coordinated and uncoordinated controls.	27
Figure 16: The output power and SOC for one disconnect/connect sequence with the coordinated and uncoordinated controllers.	28
Figure 17: The difference in the battery energy throughput for the different controllers.	28
Figure 18: Experimental coordinated control results compared to simulations of the coordinated and independent controls.	30
Figure 19: A close up of the results for Oct 25 <sup>th</sup> in Figure 18.	31
Figure 20: Example irradiance profile where the battery throughput and SOC range is reduced with the coordinated control.	32
Figure 21: Example irradiance profile where the battery throughput is reduced but the SOC range with the coordinated control.	33
Figure 22: High $P_{PV}$ variability demonstration day with the simulated difference in total battery power throughput for the two controls shown in the lowest plot.	34
Figure 23: Example irradiance profile where the battery throughput is reduced but the SOC range with the coordinated control.	34

## TABLES

Table 1: The exception and compression settings in the PNM Operations Center and MdS Aperture Center PI servers for the GE, FC, and PV active power data.	20
Table 2: BESS settings for each test.	24
Table 3: Test sequence for the two test days.	25

## NOMENCLATURE

AC	alternating current
bat	battery
BEMS	Mesa del Sol Building Energy Management System
BESS	Prosperity Battery Energy Storage System
BPF	bandpass filter
compdev	compression deviation
compmax	compression maximum
DC	direct current
excdev	exception deviation
excmax	exception maximum
FC	fuel cell
$f_{\text{High}}$	bandpass filter high frequency cutoff
$f_{\text{Low}}$	bandpass filter low frequency cutoff
GE	gas engine-generator
GE Delay	gas engine-generator control signal delay
$GE_{\text{gain}}$	proportional gain to adjust gas engine-generator use
Hz	hertz
$K_{\text{GE}}$	gas engine-generator proportional control to return the GE to the nominal power
$K_{\text{SOC}}$	battery proportional control to return the battery to the reference SOC
kW	kilowatt
kWh	kilowatt-hour
LPF	low-pass filter
MdS	Mesa del Sol
NEDO	New Energy and Industrial Development Organization of Japan
$P_{\text{bat}}$	battery power output
$P_{\text{bat-SP}}$	battery power setpoint sent to battery
$P_{\text{BPF}}$	BEMS error target from the bandpass filter
PCC	point of common coupling
$P_{\text{error}}$	difference in power between the PV power and smooth target power
$P_{\text{GE}}$	gas engine-generator power output deviation from nominal output ( $\pm 60$ kW)
$P_{\text{GE\_nom}}$	nominal gas engine-generator power (180 kW)
$P_{\text{GE-SP}}$	gas engine-generator controller setpoint sent to genset

$P_{FC}$	fuel cell power output deviation from nominal output (+30/-20 kW)
$P_{FC\_nom}$	nominal fuel cell power (50 kW)
$P_{FC-SP}$	fuel cell power controller setpoint sent to fuel cell
$P_{smooth}$	the smooth power (calculated by the low-pass filter of $P_{PV}$ )
$P_{PV}$	photovoltaic power
PNM	Public Service Company of New Mexico
PV	photovoltaic
SNL	Sandia National Laboratories
SOC	state of charge
$SOC_{ref}$	reference state of charge (e.g., $(SOC_{max} + SOC_{min})/2$ )
$T_w$	window of time for the controller moving average
$T_{Low}$	time constant associated with $f_{High}$
$T_{High}$	time constant associated with $f_{Low}$
$T_1$	BESS low-pass filter time constant
UNM	University of New Mexico
$\Delta$	change in

# 1. INTRODUCTION

Adverse impacts due to variability of renewable generation on the electrical grid are possible in cases involving weak electricity grids or high penetration scenarios. In these cases, local storage systems (e.g. batteries) can smooth the renewable power output so that the local grid voltage—and frequency in the case of island grids—are not negatively impacted. The Public Service Company of New Mexico (PNM) has a 500 kW photovoltaic (PV) system co-located with a 500 kW, 500 kWh valve-regulated lead-acid (VRLA) smoothing battery [1] at the Prosperity site near the Albuquerque Airport. The battery uses a control algorithm developed by Sandia [2, 3] to perform smoothing of the PV power. The New Energy and Industrial Development Organization of Japan (NEDO), in partnership with PNM, the University of New Mexico, and Sandia National Labs has developed a smart grid demonstration project at Mesa del Sol, to investigate building microgrid operations, integrating renewable energy generation with traditional generation, and employing storage to control PV power variability [4]. The Prosperity and Mesa del Sol projects are installed on the same 12.47 kV distribution feeder.

In previous work, the operation of the gas engine-generator (genset) and the battery was simulated to optimize the control parameters with respect to battery and inverter size, and battery lifetime [5]. In the simulations, coordinated and uncoordinated control cases were also compared. With coordinated control the battery energy management system was sent the output of the genset, so the battery could use less energy to reach the smooth power target. In the uncoordinated control, the genset and battery would smooth the PV output individually without knowledge of the output of the other system. The simulations illustrated benefits of using the coordinated control: less required battery capacity, less SOC range utilization, reduced battery amp-hour throughput, and smaller inverter size. This report describes the experimental demonstrations of the coordinated and uncoordinated control involving the PV system and battery at Prosperity and the gas engine-generator and fuel cell at Mesa del Sol. The demonstrations were designed to verify the simulations in [5], as well as experimentally quantify the benefits of employing traditional energy resources to assist battery smoothing operations.

For the demonstration, highly-controlled, repeatable PV output changes were created by disconnecting a portion of the PV array at precise times while different control algorithms were operating. Since the PV power profiles for the days were nearly identical, a direct comparison of the smoothing system operation was possible for the three cases of interest:

1. Battery smoothing only
2. Coordinated smoothing with the genset and battery
3. Uncoordinated smoothing with the genset and battery

The results of the demonstration showed a range of challenges regarding the data collection, data storage, and the exchange of data between the sites, but the behavior of the different controls matched well with the simulations and there was less battery operation when the coordinated control was implemented.

In the second test, the experimental coordinated control was compared to simulations of the coordinated and uncoordinated controllers using the same PV profile. Here the SOC range of the coordinated controller was found to be larger than the uncoordinated controller because the

genset did not return to the nominal power level for long periods of time, which biased the battery output and caused more charging in the coordinated control than the uncoordinated control simulation. This phenomenon was studied with multiple simulations using artificial PV power profiles to better understand the battery parameters of interest: the SOC range and the battery energy throughput. It was found in situations with higher variability PV power profiles, the genset is unable to return to nominal power and this causes the SOC range of the battery to drift in the coordinated control case. However, the total energy through the battery using the coordinated control was less than the uncoordinated control in all the tests and simulations. Therefore, in climates that regularly experience high irradiance variability, the coordinated control will not necessarily reduce the operational SOC range of the battery. This means that the SOC limits of the battery may be reached with the coordinated control, so alternative smoothing coordinated control parameters or control design would be advised for those PV sites.

## 2. SMOOTHING ALGORITHMS

Batteries have been used to reduce the variability of PV and wind generation in a number of studies [4, 6-9], and the coordination of renewable energy plants with energy storage continues to be an active area of research. Particularly because some island PV and wind projects are required to have energy storage systems to smooth the output variability at the point of common coupling (PCC) [10-11]; although, larger, interconnected grids do not require these systems, and it would be more cost-effective to use the energy storage system to directly maintain grid voltage and frequency [12-14]. In the case of the PNM Prosperity site, the smoothing battery was part of a larger DOE-sponsored renewable energy program and installed solely for research purposes.

For the demonstrations in Albuquerque, the Battery Energy Storage System (BESS) at the PNM Prosperity site and the Building Energy Management System (BEMS) at the Mesa del Sol (MdS) Aperture Center jointly smooth the PV output. The BESS controls the output power of the battery and the BEMS controls the output power of the genset. Each of these controllers are independent and do not know the target output power or setpoint established by the other controller.

### 2.1 Battery Energy Storage System (BESS)

The existing, operational PNM battery PV-smoothing control [2] implemented in the BESS determines the desired battery power output to meet a target output power. The BESS controller uses a moving average sliding window or low-pass filter of the PV power history to determine the target smooth power output,  $P_{\text{smooth}}$ , of the PV and battery system. In this paper a low-pass filter of 160 seconds is used. The setpoint of the battery is set to approximately the error signal,  $P_{\text{error}}$ , which is the difference between PV power output and the smooth power profile,

$$P_{\text{error}} = (P_{\text{smooth}} - P_{\text{pv}}) \cong P_{\text{bat}} \quad (1)$$

The BESS battery setpoint is not equivalent to  $P_{\text{error}}$  because there is also a return-to-nominal-SOC bias to move the  $\text{SOC}_{\text{ref}}$ . This bias is relatively small compared to battery control component tracking  $P_{\text{error}}$ , but over time it returns the energy storage SOC to a nominal value. The BESS also limits the battery to a range of within  $\text{SOC}_{\text{min}}$  and  $\text{SOC}_{\text{max}}$ , e.g., 20% and 80%, though limits will vary on the application, battery technology, and smoothing controller design. More details on the operation of the battery and the controls are provided in [5].

The BESS controller is shown in Figure 1. The green logic blocks indicate the controller installed in the BESS. The upper blocks switch between the moving average and low-pass filter. Reducing the  $G_1$  gain below 1.0 reduces the error that the battery will attempt to absorb. AUX1 and AUX2 are inputs from other sources and, for example, can include values read from other energy resources and stored in a PI historian. For all the tests, the deadband is set to zero, but could be increased to reduce the battery operations which curtail small ramp rates. The “state-of-charge tracking function” is the method that the controller returns to the reference SOC. This

loop compares the current battery SOC to  $SOC_{ref}$  and applies a small gain,  $G_4$ , to slowly bring the battery back to the reference value.

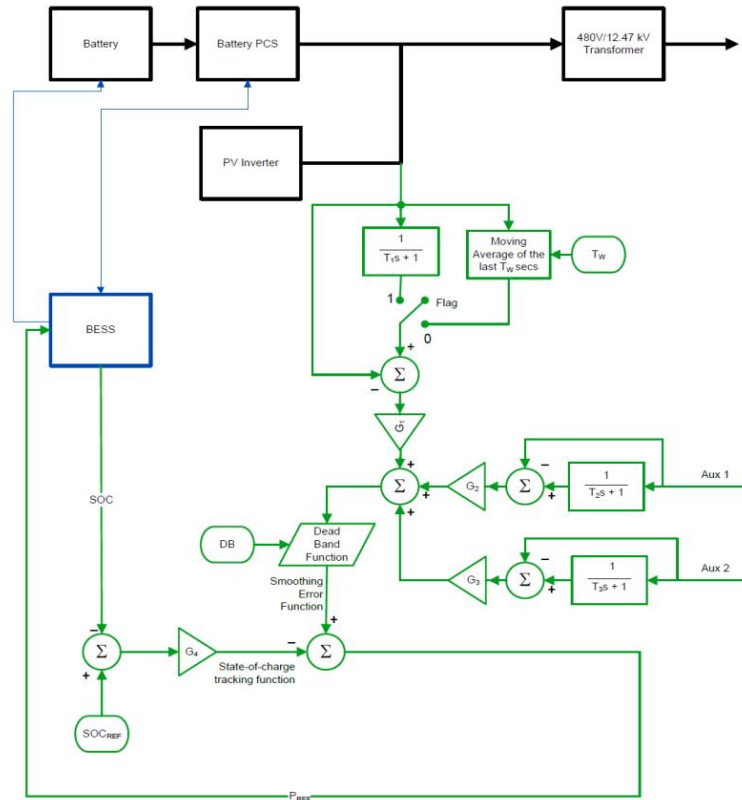


Figure 1: PNM Prosperity BESS controller [2, 3].

## 2.2 Building Energy Management System (BEMS)

The Building Energy Management System (BEMS) controls the gas engine-generator based on the output power of the Prosperity PV site. The 240 kW genset requires a minimum output of 120 kW to operate with a reasonable efficiency and emissions levels. As a result, the BEMS requires that genset operation range between 120 kW and 240 kW. The gas engine-generator is significantly slower (smaller ramp rates) than the PV and the battery, so it is only able to relieve the battery from operating during slow ramp rates. Larger ramp rates are still nearly fully tasked to the battery.

The controls system in the BEMS is shown for a system involving a gas engine-generator (GE) or “genset,” and fuel cell in Figure 2. This controller is designed so that initially the GE absorbs the entire  $P_{BPF}$  signal, but the FC setpoint is set to  $P_{GE}$  so that it can begin slowly absorbing more of the error. In the case of the demonstrations, the fuel cell is not utilized so the control in Figure 3 is used by BEMS. This controller is different than the one modelled in [5] in a couple different ways:

1. There is no loop to return the GE to the nominal output power level of 180 kW ( $P_{GE} = 0$ ).

- The control does not calculate an error signal based on the difference in PV and a smooth target; but, rather, determines the target value based on the bandpass filter of  $P_{PV} - (P_{GE} + P_{GE\_nom})$ .

The latter point is a critical one since the control implemented at MdS used a bandpass filter and the BESS used a low-pass filter. It is important to the functionality of the distributed controls to respond to the same  $P_{error}$  signal. In the simulations in this paper and in [5], the  $P_{error}$  signal is designed to be absorbed by the battery and the gas engine-generator power,

$$P_{error} = (P_{smooth} - P_{pv}) \cong P_{bat} + P_{GE} \quad (2)$$

However, in the hardware implementation, the battery and GE respond to different output targets established independently by the BESS and BEMS. Therefore, selecting settings in the BEMS and BESS were critical to ensure the coordinated control operated as the simulations expected. To do this the low-pass filter in the BESS and the low frequency value in the BEMS bandpass filter were selected to be the same, 1/160 Hz. The high frequency cutoff for the BEMS bandpass filter controller was set to  $f_{High} = 1/20$  Hz (corresponding to  $T_{Low} = 20$  seconds) so that the slow ramping GE would have the same response as it would have experienced with the  $P_{error}$  from the BESS low-pass filter. To illustrate this effect, simulations were conducted for a range of bandpass filters varying  $T_{Low}$  during a 90 kW  $P_{PV}$  step downward, shown in Figure 4. As  $T_{Low}$  decreased, the  $P_{BPF}$  signal approaches the  $P_{error}$  generated with a low-pass filter. Since the genset ramp rate is relatively slow (0.285-0.450 kW/sec depending on the genset settings) the BEMS bandpass filter and PNM low-pass filter result in the same output for the genset as long as  $T_{Low}$  is below 20 sec. Thus, as long as the Prosperity BESS  $T_1$  at BEMS  $T_{High}$  are set to 160 sec, and  $T_{Low}$  is below 20 sec, the error targets for the different controllers will be the same.

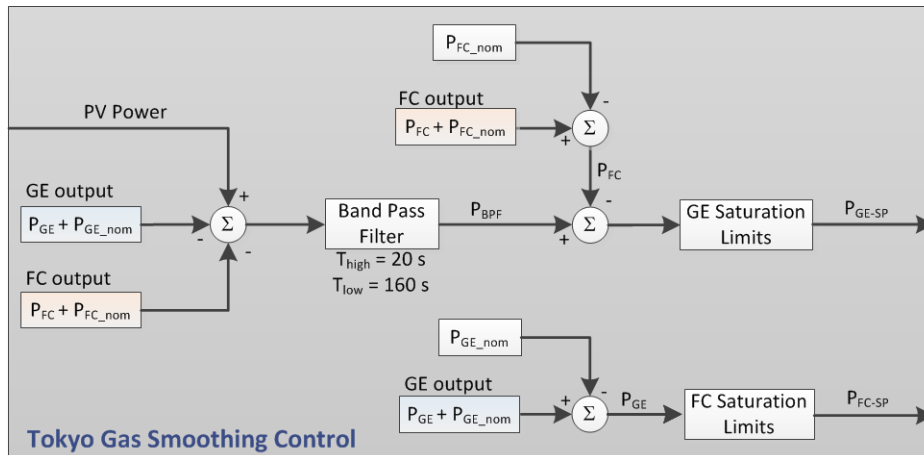


**Figure 2: MdS BEMS controller with genset and fuel cell.**

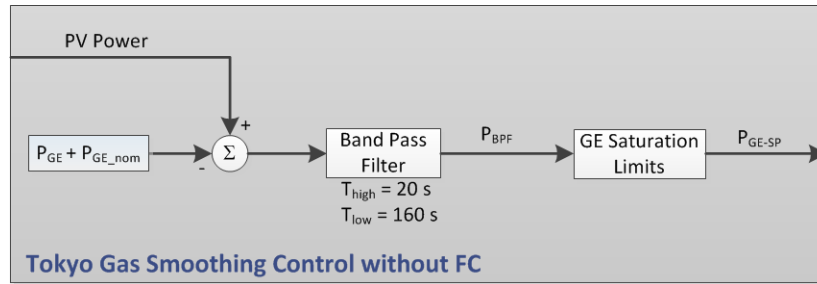


**Figure 3: MdS BEMS controller with only a genset.**

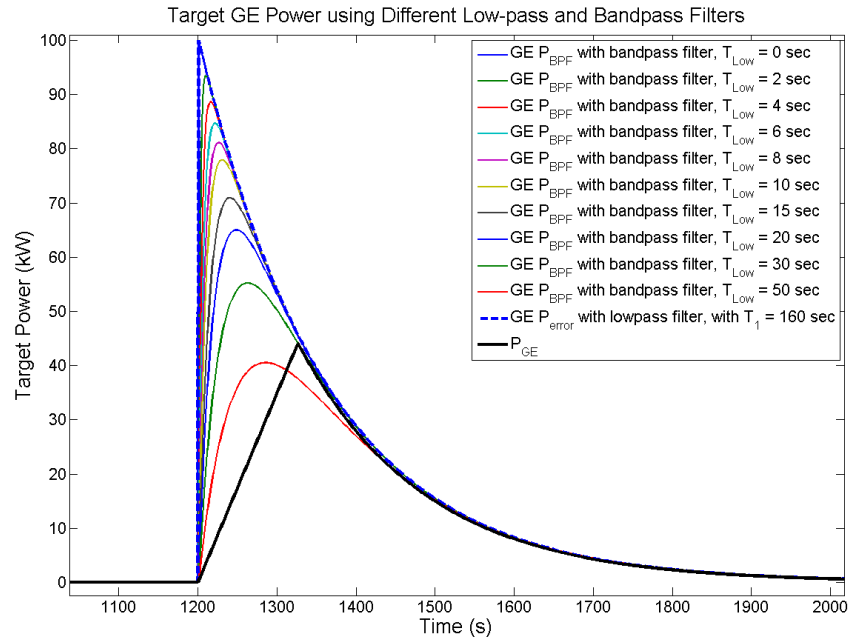


**Figure 4: Comparison of low-pass and band-pass filters. The output power from the GE will be the same when selecting  $T_1 = T_{High} = 160$  sec, and  $T_{Low} < 20$  sec.**

In order to compare the simulations shown above in Figure 4 to the true BEMS GE output target  $P_{BPF}$ , the BEMS was fed an artificial 90 kW PV power increase to verify the response of the GE setpoint and GE output power, plotted in Figure 5. The GE  $P_{BPF}$  setpoint has the expected bandpass filter curve shape, but the gas engine could not increase its output power quick enough to stay on the setpoint curve once it reached the setpoint value. This overshoot indicates the genset cannot respond as quickly as the simulations indicate due to latency or hysteresis in the control, or limitations in the physical system.

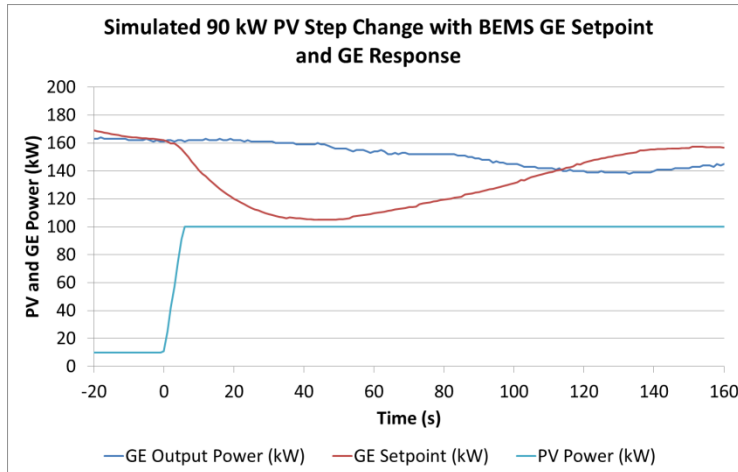


**Figure 5: The GE setpoint and active output power when a 90 kW step increase in the PV power is observed.**

### 2.3 Combined Gas Genset (BEMS) and Battery (BESS) Controllers

PV smoothing using the gas genset and battery requires simultaneous operation of the BEMS and BESS controllers. The MATLAB/Simulink models for the coordinated and uncoordinated controls of the genset and battery are shown in Figure 6. As shown in the upper grey block, the PV error signal (smoothing requirement) is calculated with a low-pass filter on the time history of  $P_{PV}$  and then transmitted to the gas engine-generator control. In reality, the calculations of  $P_{error}$  and  $P_{BPF}$  take place independently in the BESS (with a low-pass filter) and the BEMS (using a bandpass filter). However, by matching the filters (e.g.,  $T_1 = T_{High}$ ), the target output powers for the GE and battery are the same as the simulations. More details on these models are provided in [5].

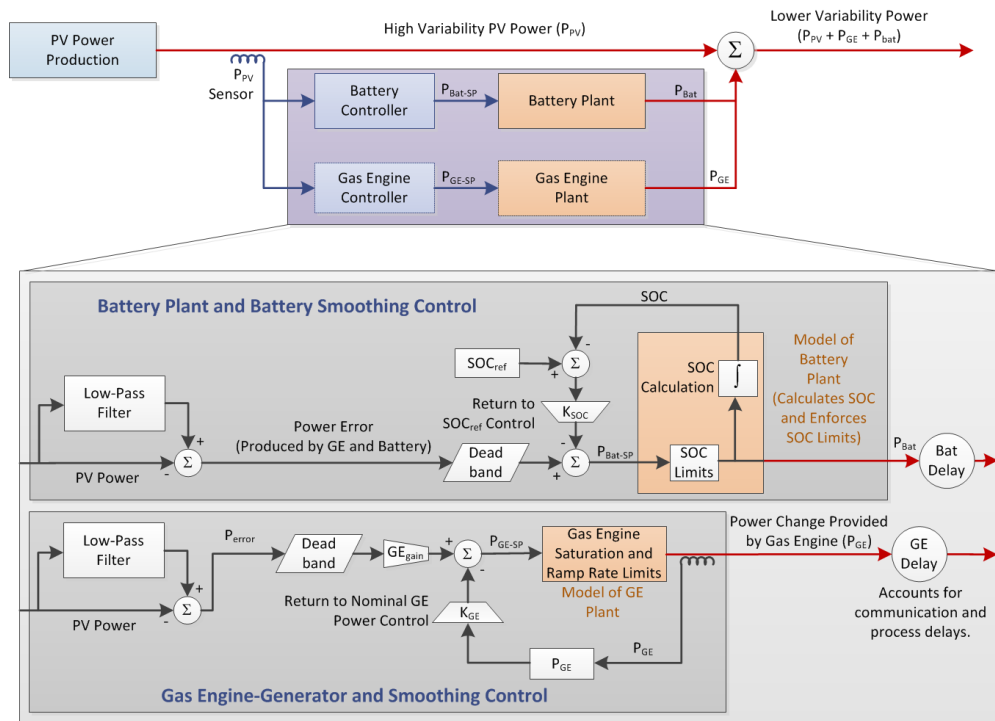
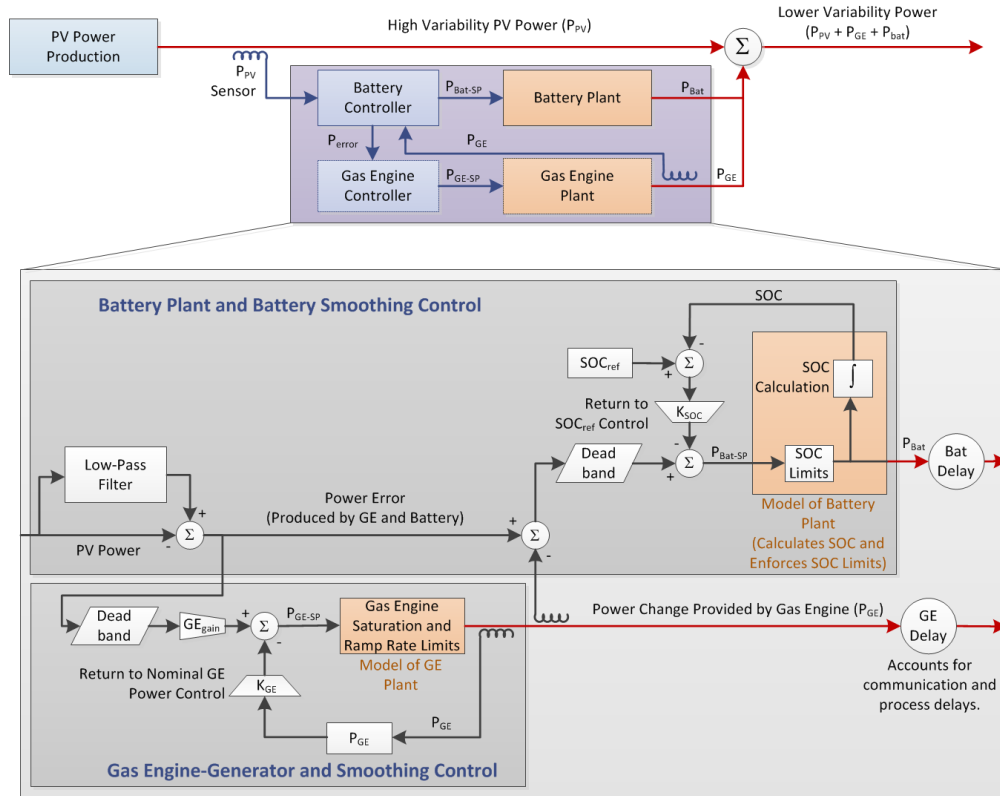


Figure 6: Control schemes for the battery and gas engine-generator.

### 3. COMMUNICATIONS

The physical separation between the Prosperity Site and the Aperture Center is roughly 2 km shown in Figure 7. This distance, along with the absence of any direct communication lines, prevented a single centralized control from coordinating the operations of the battery and genset. Instead, the information was relayed between the two sites using PI servers at the PNM Operations Center and Aperture Center.

The communications link between the PNM Prosperity BESS and Mds Aperture Center BEMS allows the coordinated and uncoordinated controls to function. Without communication between the BESS and the BEMS, the genset would be unable to compensate for the PV system fluctuations and the battery would not benefit from the genset smoothing.



Figure 7: Geographical locations of the PNM Prosperity Site and Mesa del Sol Aperture Center.

In the case of the coordinated control, information about the PV output power is sent to the BEMS and the output power of the genset is sent back to the BESS. In the case of the uncoordinated control,  $P_{GE}$  is not returned to Prosperity. The communication links for these two situations are shown in Figure 8. In both cases  $P_{PV}$  data is passed from the BESS at Prosperity to the PNM PI server located at the operations center in Albuquerque, where it is then passed to the microgrid PI server at the Aperture center through a real-time PI-to-PI interface. The  $P_{PV}$  signal is then transferred to the BEMS, which determines the gas genset setpoint,  $P_{GE-SP}$ , and sends the command signal to the genset. The output power is monitored by the BEMS and, only in the case of the coordinated control, transferred to the BESS.

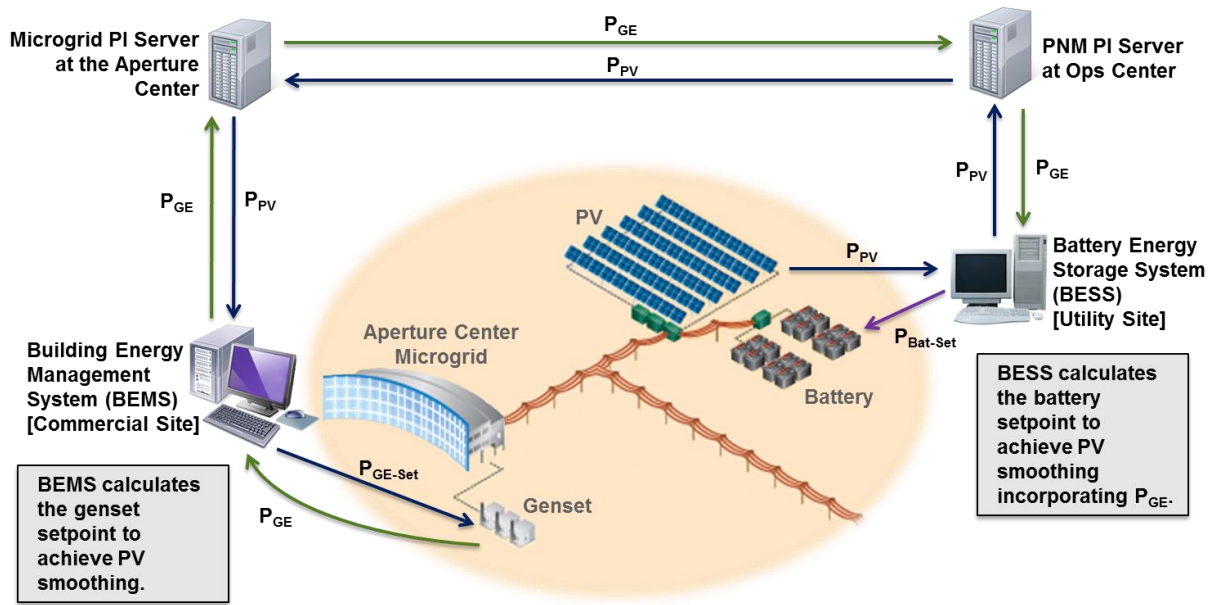
In order to accomplish the control and inform the BEMS to the status of the BESS system, the following PI tags were sent from PNM to MdS:

1. PV output power (kW)
2. Battery output power (kW)
3. Status of the smoothing battery (1 = Operating, 0 = Stopped)

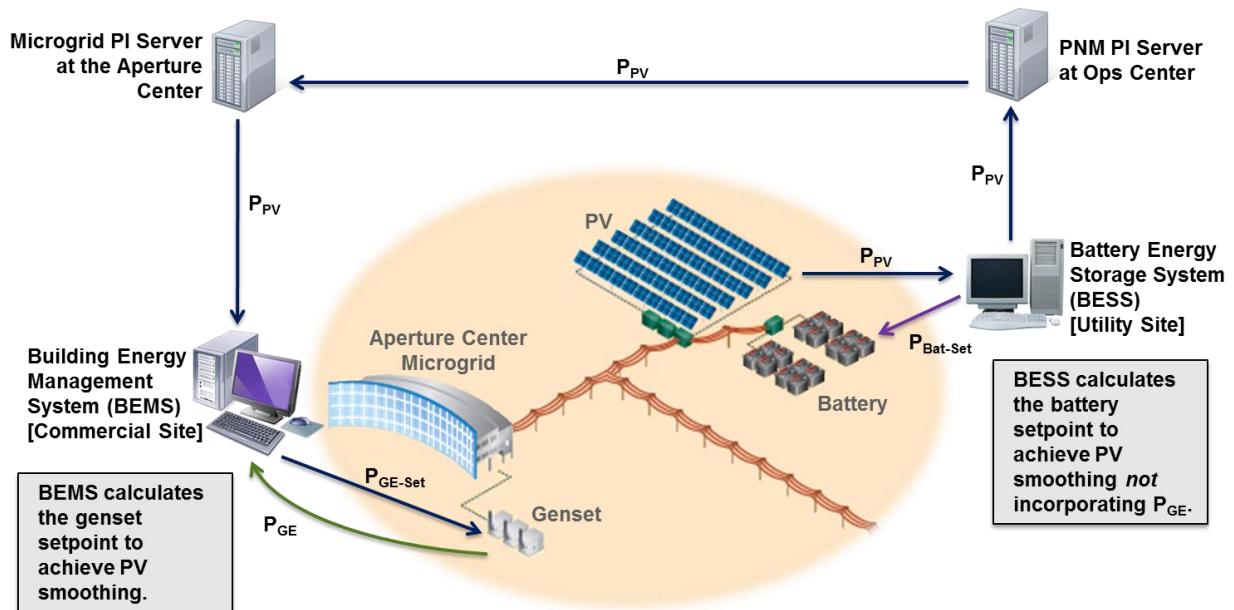
Likewise, the following PI tags were sent from MdS to PNM in order to provide information about the status and current operation of the BEMS system:

1. Gas Engine Power (kW)
2. Fuel Cell Power (kW)
3. PNM PV Power (kW) – to check communications latency
4. Status of Gas Engine (1 = Operating, 0 = Stopped)
5. Status of Fuel Cell (1 = Operating, 0 = Stopped)
6. Status of the GE & FC smoothing control (1 = On, 0 = Off)

Note that the PNM PV power was returned to the PNM server to determine the latency in the communications. The PI data (specifically PGE) was not sent from MdS to Prosperity for the uncoordinated control, as shown in Figure 8(b). The recorded data at the UNM Operations Center was sent to Sandia National Laboratories through a PI-to-PI communications link to perform the data analysis. The data sets were sampled with 1 second resolution for the analysis in this report.



(a) Coordinated Control using a PI-to-PI link between Prosperity and Mds.



(b) Independent Control of Prosperity and Mds.

**Figure 8: Control schemes for the battery/FC and gas engine-generator for Test A.**

### 3.1 Operational Historian Configuration Settings

Operational historians collect real-time measurement data and compress them into time-stamped time histories of the channels. In this demonstration, PI server historians from OSIsoft [15] were used at the Aperture Center, Prosperity Site, and Sandia in order to record and transfer data between the different locations. In general historians are designed for monitoring systems, not for real-time control. PI servers, like other industrial automation tools, compress data while it is

being collected. Therefore, not all the data sampled with a historian is saved to hard disk memory. The time history is compressed by only sending values to the PI server that exceed an *exception deviation* deadband and only saving values in the archive that exceed a *compression deviation*. The exception deviation limit is applied first and designed to reduce the communication bandwidth to the PI server by filtering out signal noise. The compression deviation reduces the required disk space required by only storing significant signal changes to the PI archive via the PI compression algorithm [16]. There is also an *exception maximum* and *compression maximum* which sets the maximum amount of time before the PI system or archive will receive a new data point if the exception or compression deviation has not been exceeded.

During the operation of the coordinated and independent (uncoordinated) controllers, the data stored on the PNM PI server was transferred to the MdS aperture center. As explained above, the exception, and compression settings must be configured correctly in order to capture significant changes in the output power from the different sources without taxing the drive space or communication channels with excessive data. The PI server settings used for the demonstration are shown in Table 1. Some tags were inadvertently left with immoderate settings, and therefore the consistency and quality of the transferred data was poor. For example, the deviation settings are clearly set too large in Figure 9, because, as the high-resolution data is transferred from the PNM PI server to MdS, there is a loss in the fidelity of the data and only a few points are collected. This compressed data is then transferred back to PNM with inappropriate attributes, illustrated by the red line in Figure 9.

**Table 1: The exception and compression settings in the PNM Operations Center and MdS Aperture Center PI servers for the GE, FC, and PV active power data.**

<i>Tag</i>	<i>excdev (kW)</i>	<i>excmax (s)</i>	<i>compdev (kW)</i>	<i>compmax (s)</i>
P <sub>GE</sub>	1	600	2	28800
P <sub>FC</sub>	1	600	2	28800
P <sub>PV</sub>	1	600	2	28800

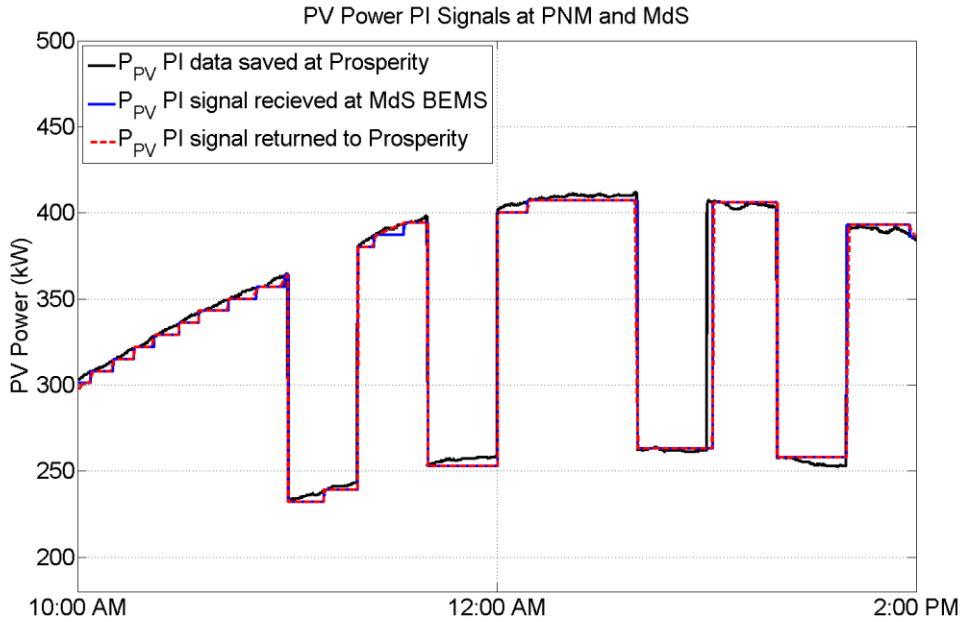


**Figure 9: Data compression and exception rules at the MdS PI server caused the step changes in the BEMS  $P_{PV}$  profile.**

### 3.2 Communications Latencies

The coordination of multiple distributed resources requires timely communication between the controllers. Latency in the communications causes the total system output to not meet the target power production, i.e.,  $P_{GE} + P_{bat}$  will not equate to  $P_{error}$  during PV power transients. In the demonstrations at Prosperity and MdS, the latency of the end-to-end communication was determined by returning the  $P_{PV}$  signal from MdS to PNM Operations Center. Therefore, the offset in the locally recorded PV power at PNM and the returned  $P_{PV}$  signal is the latency for the two transmissions:  $P_{PV}$  from PNM PI server to MdS BEMS and then  $P_{PV}$  from MdS BEMS back to PNM, shown in Figure 8(a). While the results in Figure 10 have undergone data compression and exception rules, the communication latency is approximately 1-2 seconds for each of the data transfers.

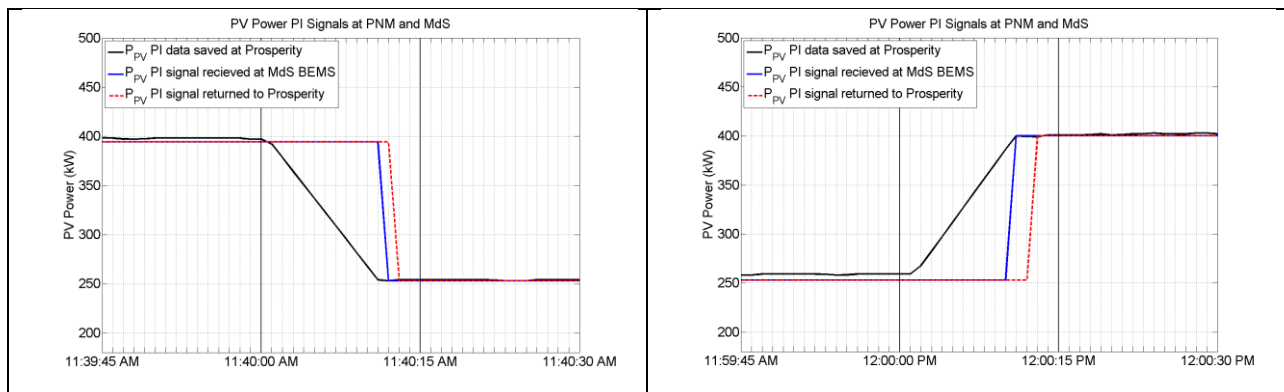


**Figure 10: Communication latency in the PI-PI link.**

### 3.3 Communication Dropouts

The PI servers transferred data continuously during the demonstrations, but there were some challenges with transferring the data from the PI server to the BEMS. The source of the communication error is unknown, but it propagated errors in the BEMS control because it would set the  $P_{PV}$  value to 0, illustrated in Figure 11. This abrupt change would result in the GE attempting to smooth an artificial, very large negative ramp rate in  $P_{PV}$ , shown in Figure 12. Fortunately, these data dropouts generally existed for a short period of time so the GE setpoint and output power were not significantly affected. In the future, logic should be built into the BEMS so that it repeats the last  $P_{PV}$  value when communications are not established between the MdS PI server and BEMS.

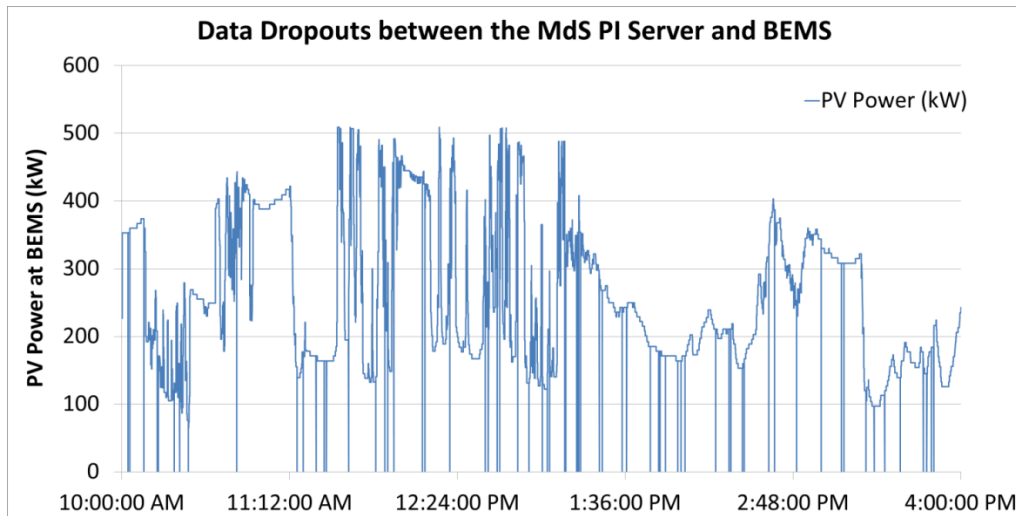


Figure 11:  $P_{PV}$  communication errors between the MdS PI server and BEMS. The dropouts occur when  $P_{PV} = 0$ .

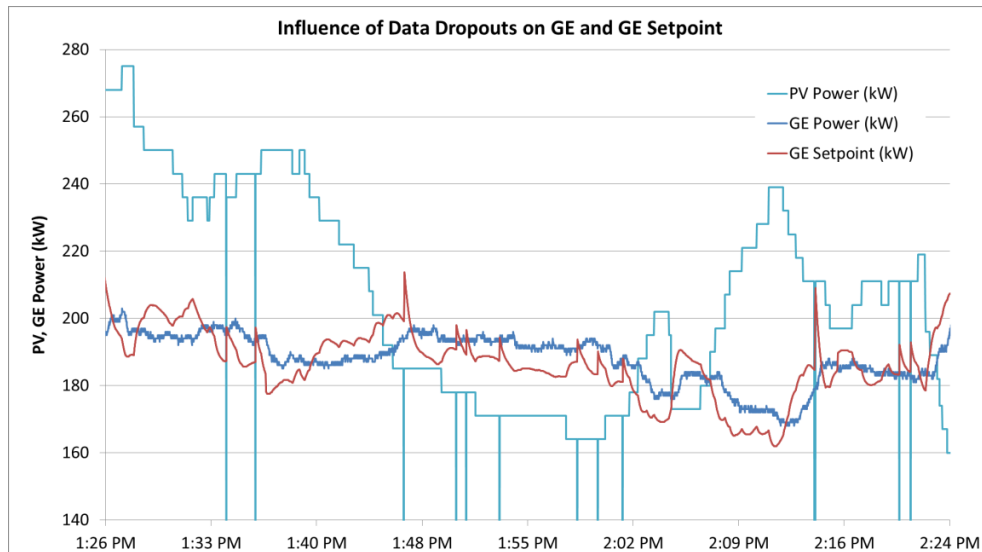


Figure 12: Gas engine setpoint and output power changes due to  $P_{PV}$  data dropouts.

## 4. EXPERIMENTAL DEMONSTRATIONS

A number of experimental demonstrations were designed to compare the coordinated and uncoordinated controllers and verify communications between Mesa del Sol and Prosperity. The primary objective of the demonstrations was to show coordinating distributed resources results in a reduction in the battery energy throughput (battery wear) and a reduction in SOC range of the battery. These benefits are the result of the GE assisting the battery smoothing—while, at the same time having little or no effect on the overall system smoothing. The two methods of comparing the control schemes were:

1. Creating highly-repeatable, artificial PV variability by switching off a portion of the PV system during subsequent cloudless days. The controlled step changes in the PV output were conducted at the same time during consecutive days to provide nearly identical input conditions for the controllers so that can be compared directly. The two data sets that are collected and compared were:
  - a. Coordinated PV output smoothing control using the Prosperity battery with assistance from a gas engine-generator while a portion of the PV array was disconnected.
  - b. Uncoordinated PV output smoothing using the Prosperity battery with independent (uncoordinated) assistance from the GE.
2. Recording the coordinated smoothing algorithm during a day with variable irradiance (partly cloudy weather). Then, comparing this result to the coordinated and uncoordinated simulations by replaying the  $P_{PV}$  into the Simulink simulation. The three data sets from this test were:
  - a. The real-time coordinated controller results for a variable PV day.
  - b. The simulated coordinated controller results for the same day, in which the PV power is replayed into simulation.
  - c. The simulated uncoordinated controller results for the same day, in which the PV power is replayed into simulation.

There were also plans to compare the results of Test 2a to experimental results, but time did not permit this experiment. In that test, the uncoordinated battery operation would be experimentally determined for the same cloudy day in Test 2a by replaying the PV output data from Test 2a into the BESS AUX1 with the PV gain,  $G_1$ , turned off. The operation of the battery during this test could then be added to the recorded GE output to get the experimental results of the uncoordinated results. Essentially, this is a method to experimentally compare results from 2a to uncoordinated control results:

- d. The real-time experimental operation of the battery is determined by replaying the PV profile from 2a into the AUX port of the BESS. The  $P_{bat}$  results are then added to  $P_{GE}$  from 2a to determine the overall uncoordinated system power output.

Please note that in Test 1, the results from the battery operating alone can be determined from the uncoordinated control by removing the operation of the GE.

## 4.1 Experimental Setup

The settings in BEMS and BESS were selected to demonstrate the differences in the coordinated and independent controllers. Originally the Fuel Cell at the Aperture Center was going to be included in the smoothing operations, but it experienced a critical error and was not available for the comparison. The genset ramp rate limits were also expanded from those in [5] to the experimentally-determined maximum ramp rate of  $\pm 0.326$  kW/second to better demonstrate the differences in the controls. The BESS  $T_1$  control parameter was selected for each test to match the BEMS settings. The other BESS control settings are shown in Table 2.

**Table 2: BESS settings for each test.**

Symbol	Name	Units	Test 1a	Test 1b	Test 2a	Test 2d
Test Description			Real-time, Coordinated, Clear day, DC switching	Real-time, Uncoordinated, Clear day, DC switching	Real-time, Coordinated, Cloudy day, (Record $P_{GE}$ )	Replay 2a, Uncoordinated, Cloudy day, (Not completed for this report)
$T_W$	PV Moving Average Time Window	seconds	N/A	N/A	N/A	N/A
$T_1$	PV Low Pass Filter Time Constant	seconds	160*	160*	160*	N/A
$T_2$	AUX1 ( $P_{FC} + P_{GE}$ ) Low Pass Filter Time Constant	seconds	$1 \times 10^6$	N/A	$1 \times 10^6$	N/A
$T_3$	AUX2 (PV Replay) Low Pass Filter Time Constant	seconds	0	0	0	160*
Flag	Switch between LPF and MA	0 = MA 1 = LPF	1	1	1	1
$G_1$	PV Smoothing Error Gain	unitless	1	1	1	0
$G_2$	AUX1 ( $P_{FC} + P_{GE}$ )	unitless	1	0	1	0
$G_3$	AUX2 (PV Replay)	unitless	0	0	0	1
$G_4$	SOC Tracking Gain	unitless	10**	10**	10**	10**
DB	Dead Band Width	kW	0	0	0	0

\* Selected to match the BEMS bandpass filter.

\*\* The return-to-SOC<sub>ref</sub> gain was set to a small value so it would minimally influence the tests because the initial SOC point of the tests could not be guaranteed.

## 4.2 Real-time Demonstration of Coordinated and Uncoordinated Control with Artificial PV Variability

In October 2013, experimental demonstrations of the different controllers were performed with a team of members from Sandia, PNM, Shimizu, Tokyo Gas, and Toshiba. The purpose of these tests was to demonstrate the technical feasibility of achieving real-time coordinated operation of the Prosperity and MdS sites. Another objective was to measure the benefits of coordinated control compared to independent control with respect to key performance parameters, including battery state of charge, battery energy throughput, smoothed PV output, and maximum battery PCS output.

On two consecutive clear days, two of the DC combiner boxes of the Prosperity PV array were disconnected and re-connected as drawn in Figure 13. The test sequence for the two test days is shown in Table 3. On the first day, the control was coordinated in the morning and independent in the afternoon. On the second day, the control was independent in the morning, and coordinated in the afternoon. The tests were switched at approximately 12:20pm so atmospheric differences (humidity, pollution, etc.) between days would not influence the results. The variability in PV output due to these conditions is shown in Figure 14.

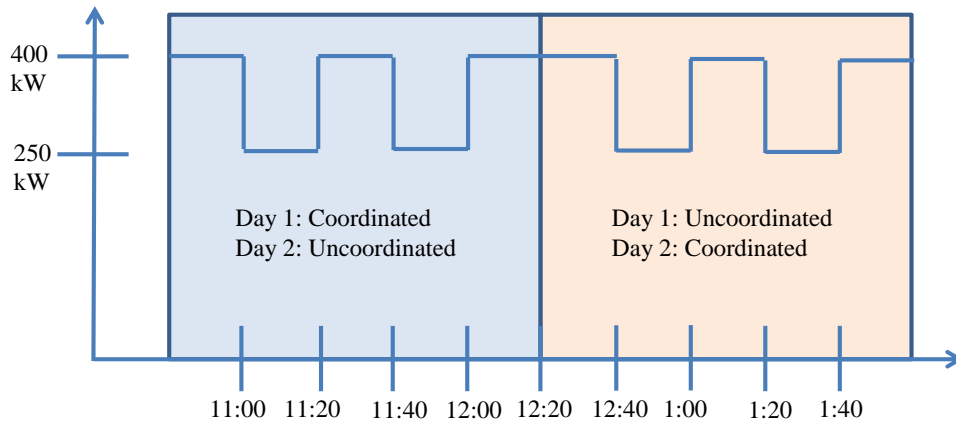


**Figure 13: Test procedure for the real-time PV output step change.**

**Table 3: Test sequence for the two test days.**

Test Sequence Day 1	Test Sequence Day 2
10:00 G2 = 1 (Coordinated)	10:00 G2 = 0 (Uncoordinated)
11:00 Switch PV off	11:00 Switch PV off
11:20 Switch PV on	11:20 Switch PV on
11:40 Switch PV off	11:40 Switch PV off
12:00 Switch PV on	12:00 Switch PV on
12:20 G2 = 0 (Uncoordinated)	12:20 G2 = 1 (Coordinated)
12:40 Switch PV off	12:40 Switch PV off
13:00 Switch PV on	13:00 Switch PV on
13:20 Switch PV off	13:20 Switch PV off
13:40 Switch PV on	13:40 Switch PV on

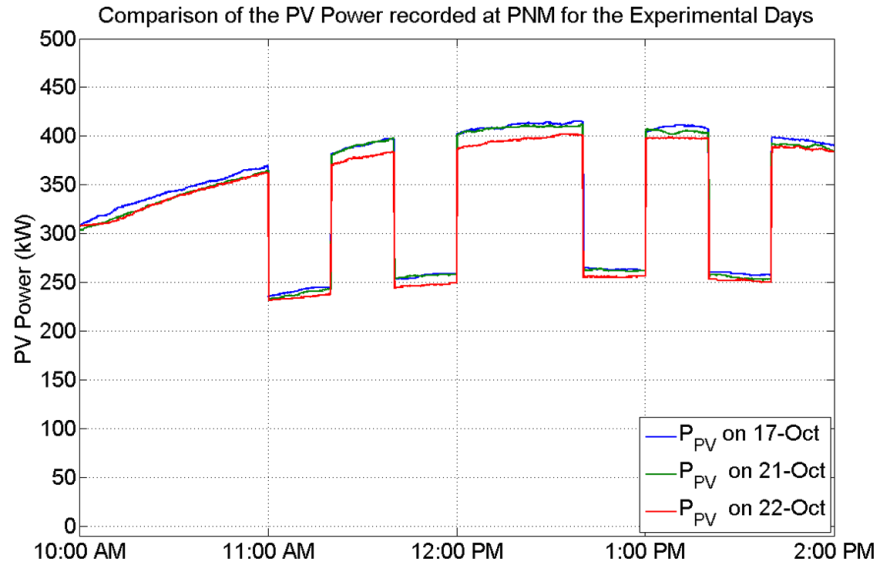


**Figure 14: PV power variability between tests days.**

Simulations were performed for the coordinated and uncoordinated controllers to determine the expected battery and genset output for given  $P_{PV}$  profiles (Figure 14). Results from Oct 21 and 22 were used for the comparative analysis and shown in the top plot of Figure 15. As the  $P_{PV}$  power drops rapidly at 11:00 AM, the bandpass filter in the BEMS and the low-pass filter in BESS determine the setpoints for the battery and GE. The simulations show with the uncoordinated controller, the GE and battery respond independently so there is no adjustment in  $P_{bat}$  as the GE ramps up. For the coordinated control, however, the BESS receives  $P_{GE}$  (blue line) via AUX1 and tapers the battery output according to the genset power (black line). This trend can be seen in each of the step changes in the simulation results in Figure 14.

The results of the demonstrations do not match the simulations closely. The battery in the coordinated control on Oct 21 was charging in order to return to  $SOC_{ref}$  so there is a clear negative shift in  $P_{bat}$  (black line) in the morning. Additionally, while the deadband in the BESS controller was set to 0, something caused  $P_{bat}$  to sharply return to 0 at around  $P_{bat} = 25$  kW. The other strange behavior is when the  $G_2$  gain is changed to turn on or off the coordinated control, there is a sudden change in the battery output.  $G_2$  is read from a PI tag at the PNM Operation Center, so it was believed this sudden change in  $P_{bat}$  could be caused by transient values being read from the PI tag while it is being changed. As can be seen from the demonstration results, the best comparison between the coordinated and uncoordinated controllers was between 1:20 PM and 1:40 PM. These switching events are analyzed in more detail below.

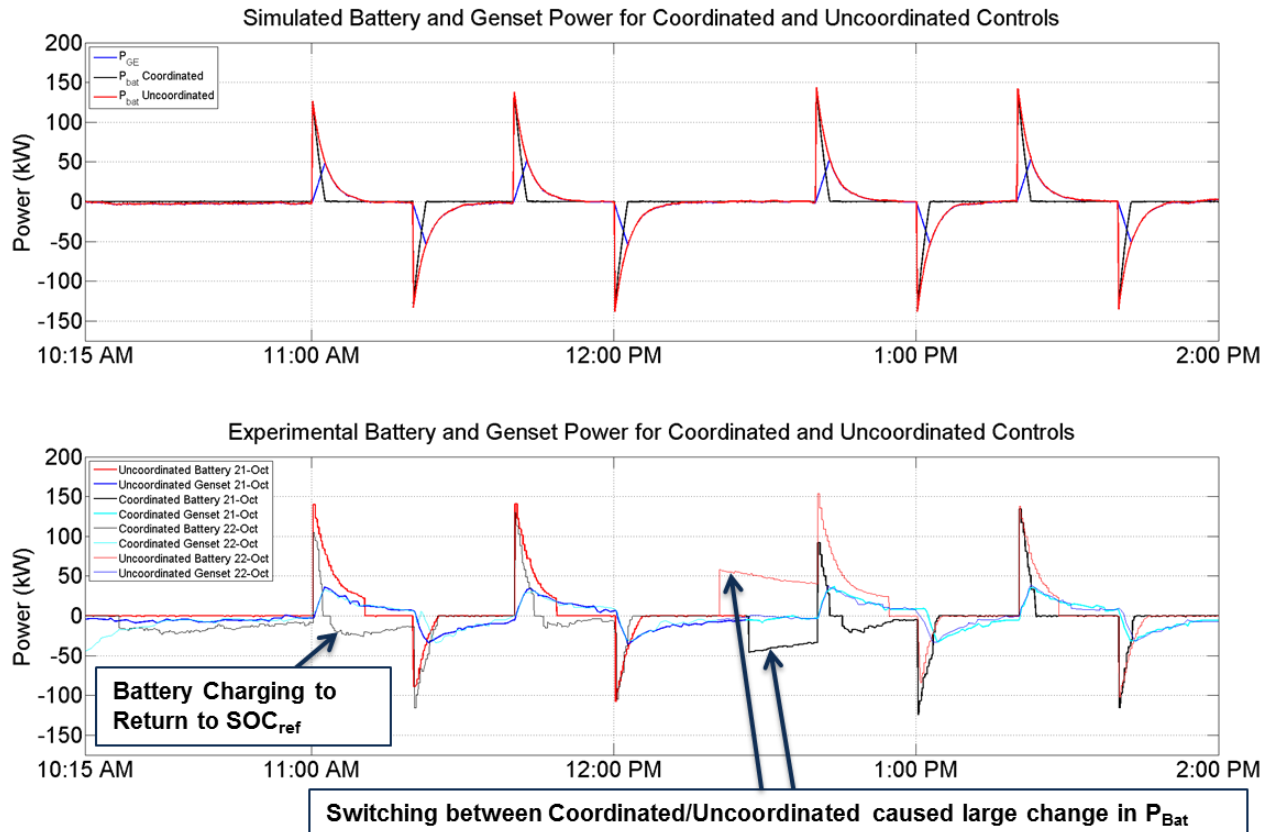


**Figure 15: Simulation and experimental results for battery and gas engine output power for coordinated and uncoordinated controls.**

The time period between 1:10 PM and 2:00 PM did not experience any transient effects from changing the control parameters or a  $P_{bat}$  offset from the SOC return signal. Therefore, this region was investigated in more detail in Figure 16. As shown in the top figure, the PV power was stepped down at 1:20 PM and up at 1:40 PM. The top figure also shows that the smooth power target is reasonably well matched by the total power from the system for both the coordinated and uncoordinated controls. In the middle figure, the experimental coordinated and uncoordinated genset output powers are very similar, as expected, since they are solely a function of the PV power profile. However, the simulations over-predict the  $P_{GE}$  ramp rates, and the experimental results are less capable of reaching the target output or returning to nominal output in short periods of time. The uncoordinated battery exports more energy for both the PV step down and up than the simulation, possibly because the SOC is above the reference value. The coordinated battery power is larger than the simulation during the down-step but larger during the up-step in  $P_{PV}$ . In both steps, the coordinated control battery exports and imports less energy than the uncoordinated control battery. As a result, the SOC range utilized by the coordinated battery is less than the uncoordinated battery, shown in the bottom plot. The SOC changes do not perfectly match the simulations, but the overall trend is the same. The positive bias on the coordinated  $P_{bat}$  means that the SOC does not return to 0 at 2:00 PM. In the upper figure, the summation of the DER powers is shown with the  $P_{smooth}$  target. In both control cases, the smooth output has much smaller ramp rates than  $P_{PV}$  and the total output power closely matches the target low-pass filter output.

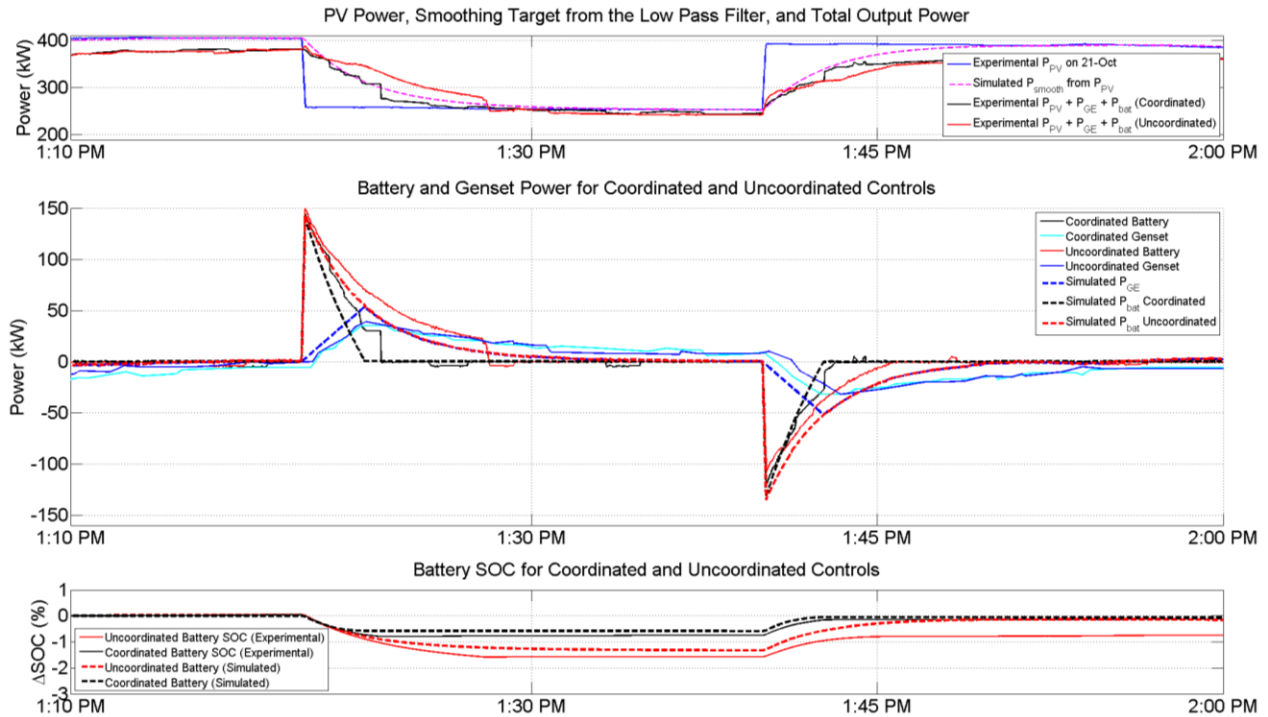


**Figure 16: The output power and SOC for one disconnect/connect sequence with the coordinated and uncoordinated controllers.**

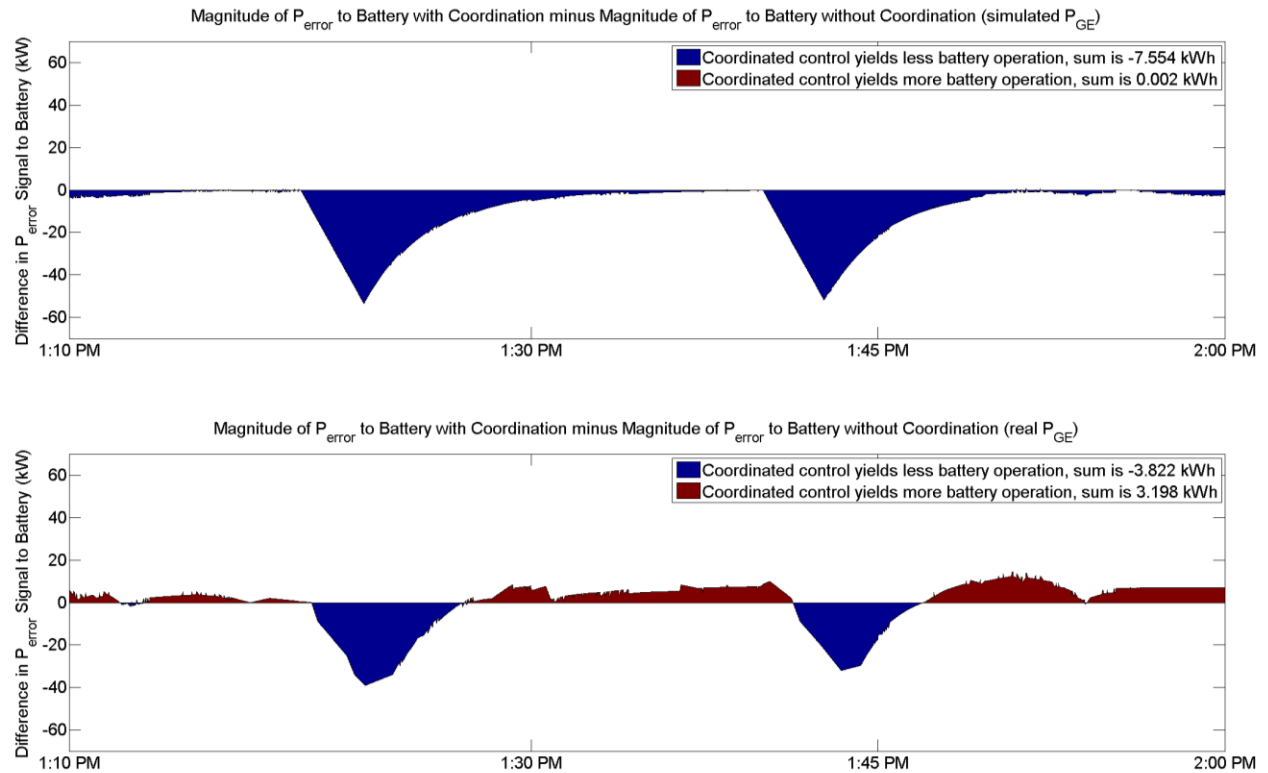


**Figure 17: The difference in the battery energy throughput for the different controllers.**

The other figure of merit for the control scheme is the total energy or amp-hours that are charged and discharged by the battery. This parameter indicates how much wear is put on the battery, which is a good estimate for the lifetime of the hardware. To determine how much less wear the coordinated control places on the battery, the  $P_{\text{error}}$  signal magnitude (i.e., amplitude of the charge and discharge command) to the battery is calculated for the coordinated and uncoordinated control. The coordinated control battery error signal is  $P_{\text{error}} - P_{\text{GE}}$  and the uncoordinated control battery error signal is  $P_{\text{error}}$ . In cases where the GE is reducing the  $P_{\text{error}}$  signal the battery does not work as much; but, at times  $P_{\text{GE}}$  is the opposite sign of  $P_{\text{error}}$  and the battery is working harder in the coordinated control scheme. By subtracting the battery error signals for the coordinated and uncoordinated controls, the improvement in the battery life can be estimated. In Figure 17, the difference in the coordinated error signal to the uncoordinated error signal is plotted for the same time period shown in Figure 16. The upper plot shows the simulated difference in the errors reaching the battery, which should be nearly the same as the difference in the actual  $P_{\text{bat}}$  depending on the return to  $\text{SOC}_{\text{ref}}$  loop control. As shown in the figure, nearly the entire time, the simulated coordinated controller is reducing the power provided by the battery. For this 50 minutes, the total energy throughput reduction from using the coordinated controller is 7.554 kWh, whereas only 0.002 kWh of the battery throughput is required using the coordinated control when the GE was working against the battery (i.e.,  $P_{\text{GE}}$  and  $P_{\text{error}}$  were different signs). Unfortunately, when this result is compared to the actual  $P_{\text{GE}}$  output in the lower plot of Figure 17, the  $P_{\text{GE}}$  does not follow the simulation well and the coordinated control only provides a slight advantage over the uncoordinated control. The area indicated in red is the period of time where the battery was forced to work harder to provide smooth power because  $P_{\text{GE}}$  was increasing error signal to the battery.

However, in general, the battery and GE simulation results match the trends of the experimental results. The overall benefits from the coordinated controller over the uncoordinated controller are illustrated in the simulated and experimental results in Figure 16 and Figure 17. Namely, the total power through the battery and the SOC range of the battery were reduced when the coordinated controller was implemented, while still providing similar levels of PV smoothing. By reducing the SOC range used by the battery, there is less chance the battery will reach the SOC limits, and in future designs a smaller battery could be used for the same application. Reducing the total energy, e.g., amp-hours, reduces the wear on the battery and extends the life expectancy of the hardware.

### 4.3 Comparison of real-time coordinated control to simulated controllers

The artificial PV variability from disconnecting a portion of the PV array was an excellent method of experimentally comparing the control algorithms, but it did not capture the true range of ramp rates caused by natural irradiance. In order to better understand the behavior of the control algorithms for a high-variability days, the coordinated controller was run for a partially cloudy day. The results from the demonstration were then compared to the simulations for the coordinated and uncoordinated controls. The behavior of the battery with and without the assistance of the GE can be seen in the difference of the simulated controllers. Further, the

accuracy of the simulation can be determined based on the difference in the experimental coordinated demonstration and the simulated coordinated controller.

The coordinated experimental results and simulations for the high variability day are shown in Figure 18. On this particular day, some battery cells experienced (typically rare) over-voltage errors because of extremely large PV power ramp rates. The first over-voltage error shut down the battery at 10:13 (eventually reset at 10:46 AM) and the 2<sup>nd</sup> one occurred during the large PV ramp at 12:20 PM (but was reset within 5 minutes). For the remainder of the day, there were other faults, but these were corrected in less than 1 minute.

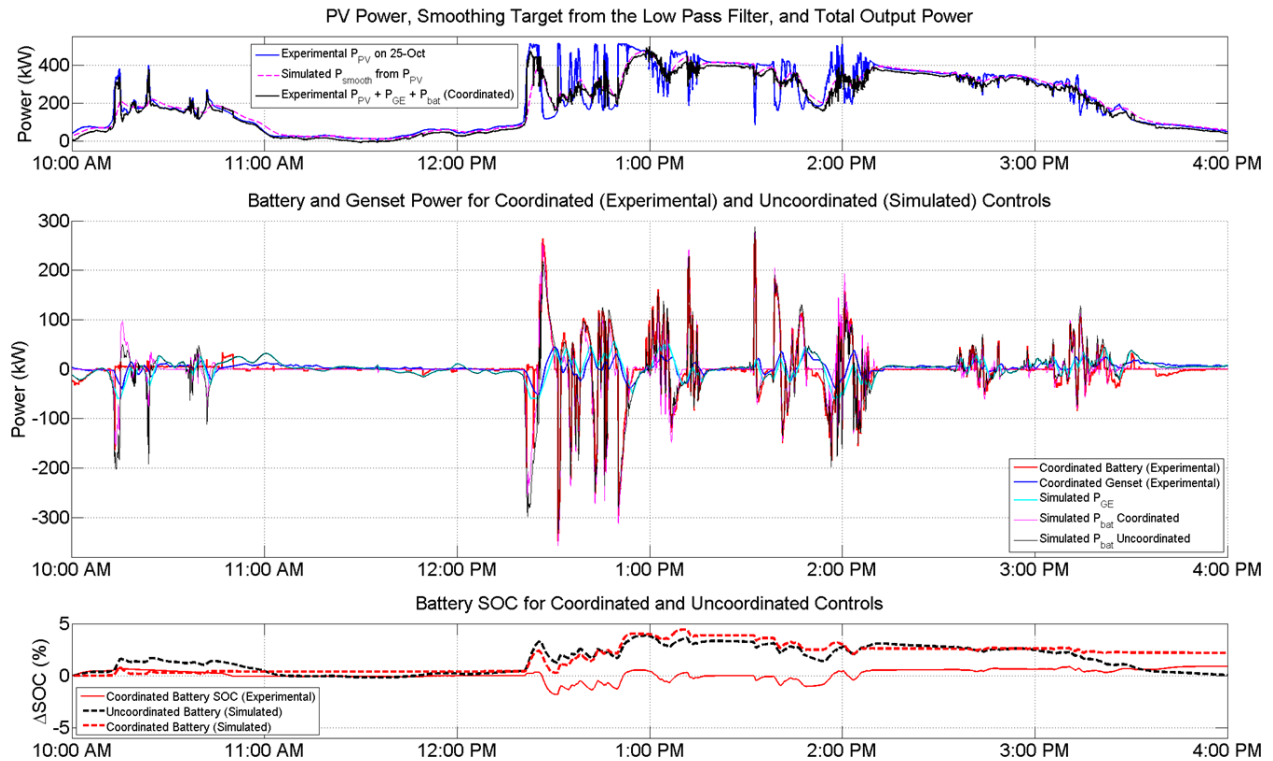


**Figure 18: Experimental coordinated control results compared to simulations of the coordinated and independent controls.**

For this particular day, the SOC range of the coordinated controller was larger than the uncoordinated controller because the high variability of the irradiance did not allow the GE to return to  $P_{GE\_nom}$ . The effect can be seen in Figure 19, where  $P_{GE}$  remains above zero for an extended period and therefore the battery error (i.e.,  $P_{error} - P_{GE}$ ) is biased negative and the coordinated  $P_{bat}$  is more negative (charging) than  $P_{bat}$  for the uncoordinated controller. This results in the SOC for the coordinated controller increasing more over that time period than the uncoordinated controller.

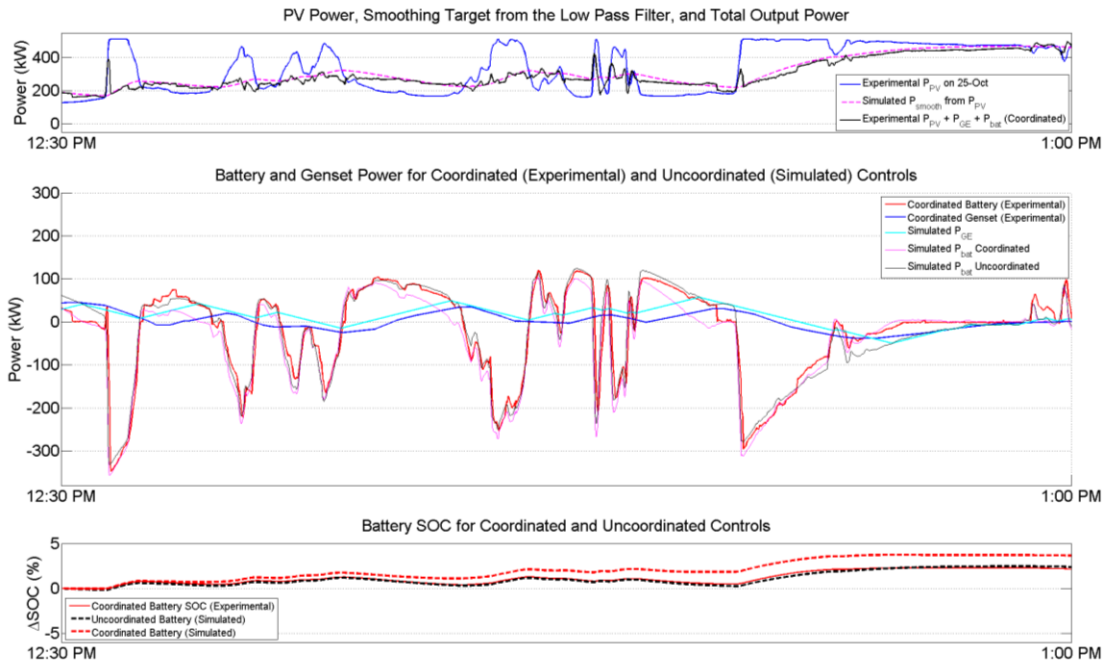


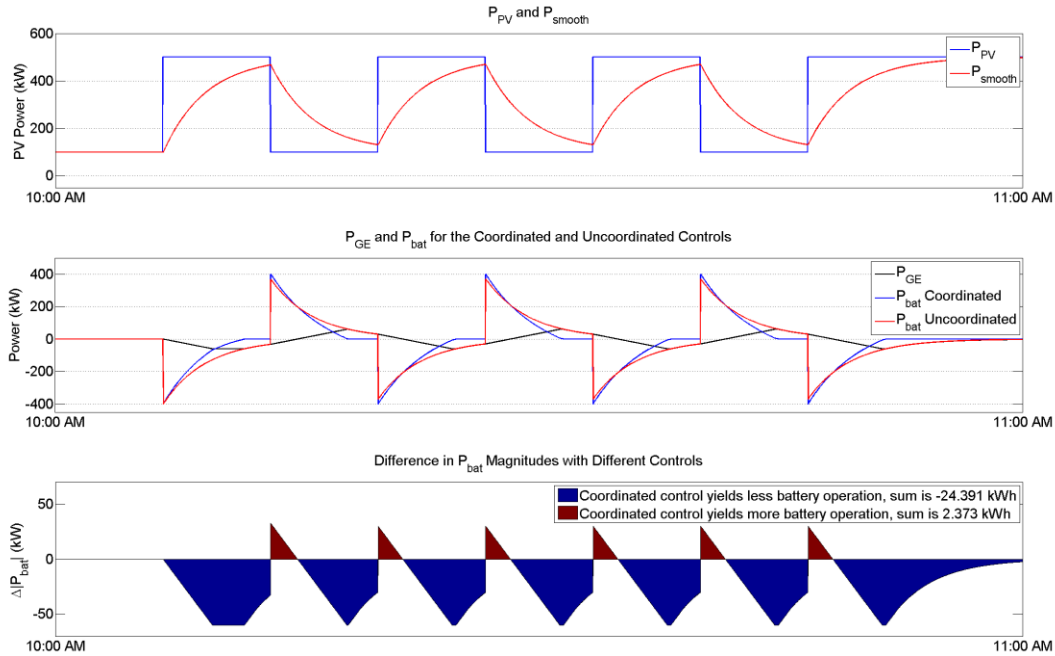
**Figure 19: A close up of the results for Oct 25<sup>th</sup> in Figure 18.**

The SOC range on the high variability day was larger with the coordinated control than uncoordinated because  $P_{GE}$  remained positive for a long period which biased  $P_{bat}$  negative. However, the total battery power throughput (charged or discharged) was reduced with the coordinated controller. To illustrate these effects in high variability situation two PV power profiles were simulated with the controllers. Each profile was a 400 kW amplitude square wave, but the first one (shown in Figure 20) has a period of 800 seconds, whereas the second profile (Figure 21) has a period of 120 seconds.

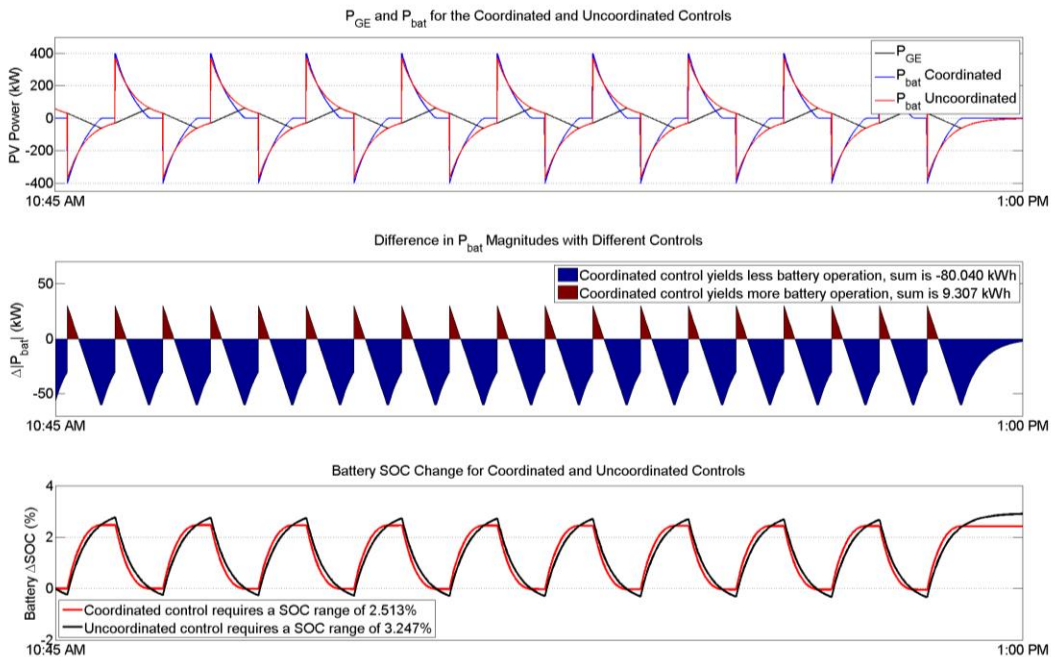
In the case of the square wave with a longer period, the battery nearly recovers to  $P_{GE\_nom}$  before the next step change occurs, so there is only a small amount of time that the  $P_{bat}$  and  $P_{GE}$  have different signs. When  $P_{bat}$  and  $P_{GE}$  have different signs the coordinated controller works harder to make up for the GE power to reach  $P_{smooth}$ . This is shown in lower plot of Figure 20(a) where the blue area shows times where the battery is helped by the GE. The red region is the time period where  $P_{GE}$  and  $P_{bat}$  have different signs and the battery is working harder with the coordinated controller. In these simulated results, the battery power,  $P_{bat}$ , is assumed to be the same as the error signal reaching the battery ( $P_{error} - P_{GE}$ ). This ignores the small signal returning the battery to  $SOC_{ref}$ . In the Figure 20(b), a longer duration of the square wave is plotted and the SOC range is shown in the lowest plot. In this case, since the  $P_{GE}$  is operating around zero, the coordinated control reduces the SOC range utilized by the battery to reach the  $P_{smooth}$  target.

With the higher variability (smaller square wave period) simulation in Figure 21, the GE does not help the battery as much as in Figure 20. In fact, the battery is *fighting* the GE (i.e. they have different signs) nearly half the time so the total energy passing through the battery is nearly the same with the coordinated and uncoordinated control, because the red and blue areas are nearly the same in the lower plot of Figure 21(a) and middle plot of Figure 21(b). Although, there is no irradiance profile that would result in the coordinated battery energy throughput being larger

than the uncoordinated control. In this simulation there is another difficulty with the coordinated control however. The GE is operating below zero for the majority of the simulation, so  $P_{bat}$  is more positive (discharging) with the coordinated control methodology, and therefore the SOC range of the battery is biased negatively, as shown in the lower plot of Figure 21(b). This leads to a much larger SOC usage with the coordinated control compared to the uncoordinated control.

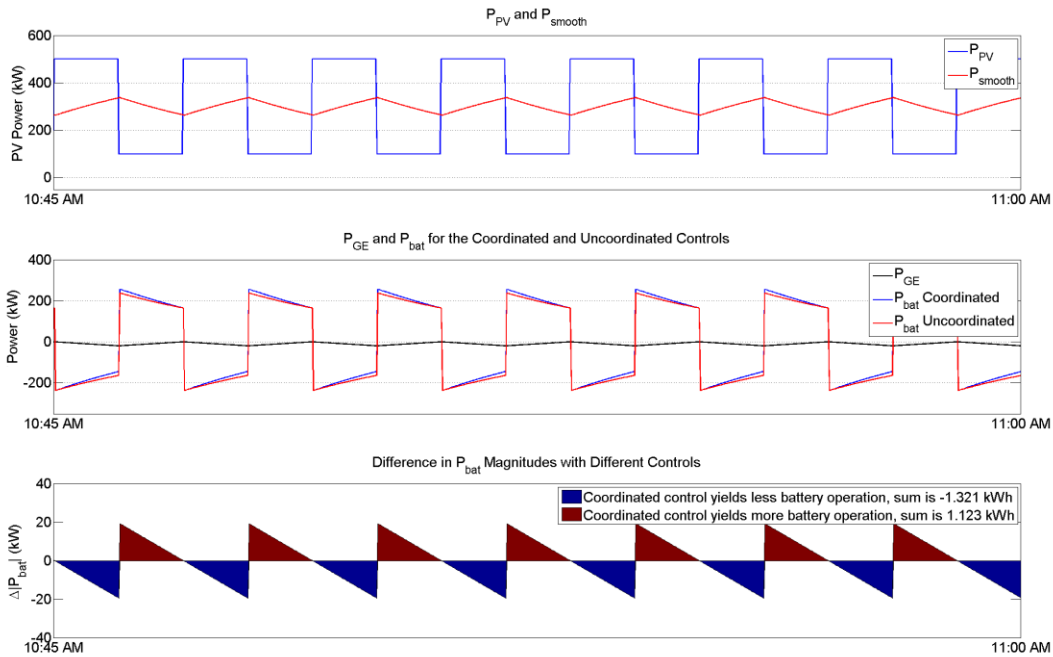


(a) Comparison of the battery energy throughput between coordinated and uncoordinated controls.

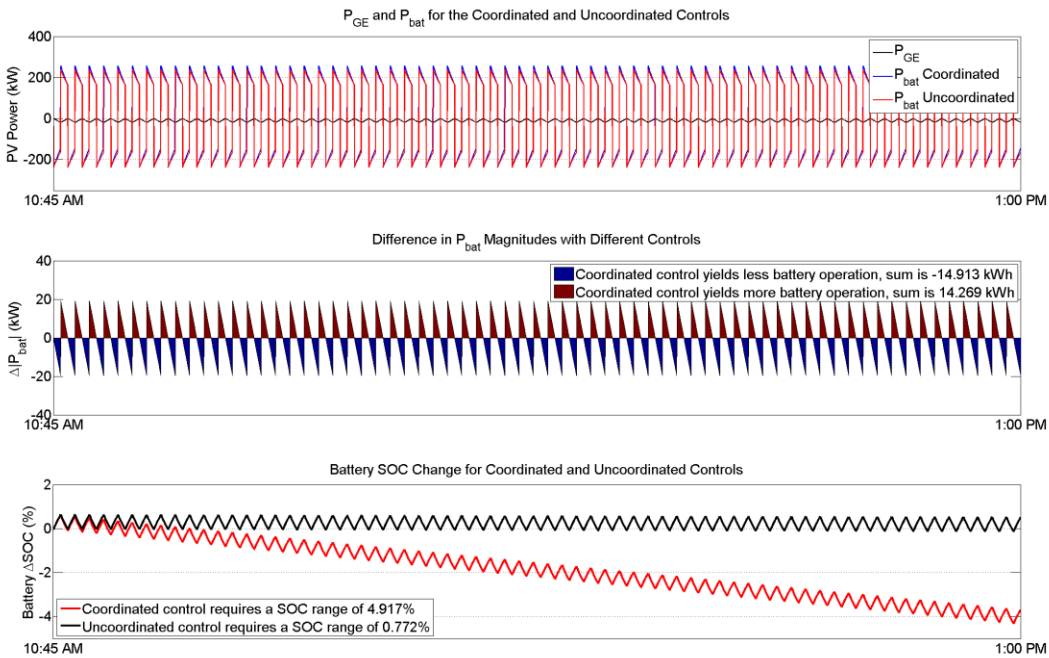


(b) Comparison of the battery SOC between coordinated and uncoordinated controls.

**Figure 20: Example irradiance profile where the battery throughput and SOC range is reduced with the coordinated control.**



(a) Comparison of the battery energy throughput between coordinated and uncoordinated controls.



(b) Comparison of the battery SOC between coordinated and uncoordinated controls.

**Figure 21: Example irradiance profile where the battery throughput is reduced but the SOC range with the coordinated control.**

This method of analysis was applied to the results of the high variability test day. The simulation results indicate the total wear on the battery, as predicted by amp-hour throughput, is reduced with the coordinated control, illustrated in the lowest plot in Figure 22. The simulated error reaching the battery was compared to the experimental, in Figure 23. It appears the GE is

slower, has more hysteresis, or cannot hit the same setpoint as in the simulations because the battery operational energy usage is only improved by 24.88 kWh in the experiment—compared to a theoretical 60.17 kWh in the simulated results—when switching to the coordinated controller.

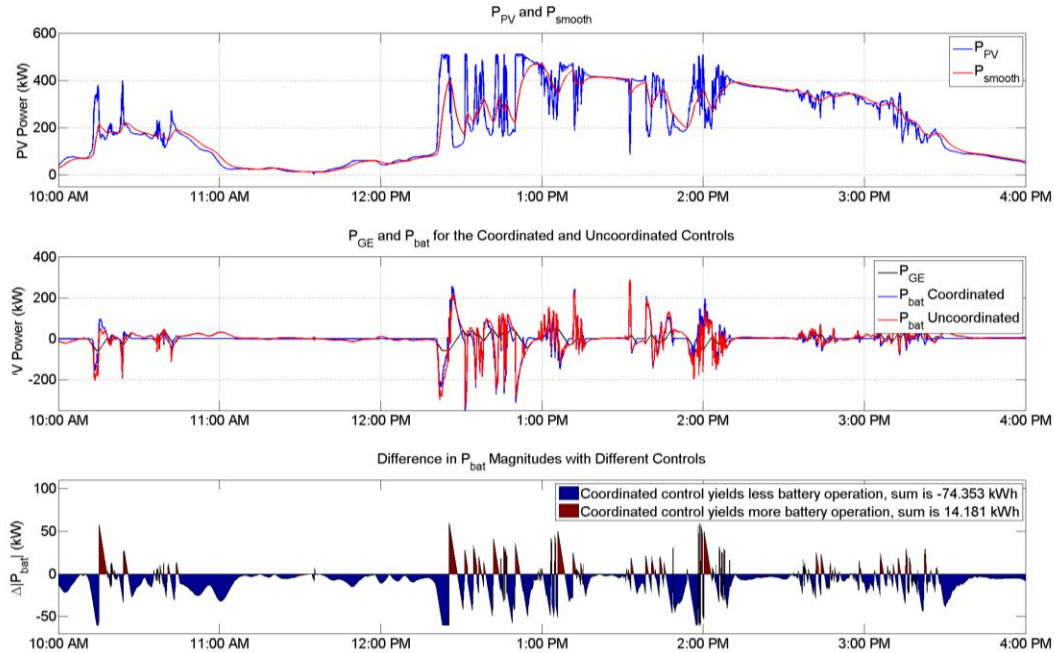


**Figure 22: High P<sub>PV</sub> variability demonstration day with the simulated difference in total battery power throughput for the two controls shown in the lowest plot.**

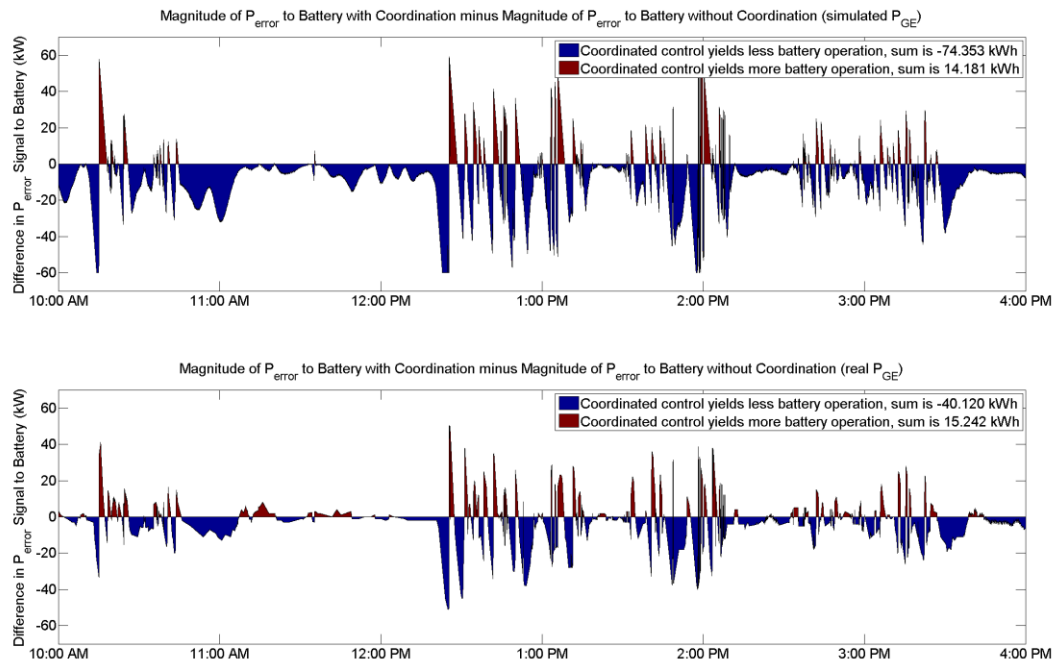


**Figure 23: Example irradiance profile where the battery throughput is reduced but the SOC range with the coordinated control.**

## 5. CONCLUSIONS

Previously, simulations of PV power smoothing control strategies at Prosperity and Mesa Del Sol were performed in MATLAB/Simulink to demonstrate that using traditional energy sources, in addition to a battery provides a number of benefits, including longer battery life and smaller required battery capacity. These controllers were demonstrated in the field with a 500 kW PV system, 500 kW lead acid smoothing battery, and a 240 kW gas engine-generator. In order to perform the tests, communications were established between the Battery Energy Storage System (BESS) and the Building Energy Management System (BEMS) at the MdS Aperture Center with OSIsoft PI historians through a PI-to-PI tag exchange. This method of communicating was difficult because there are a number of exception and compression settings on the data prior to being stored on the servers. Historians are not designed for real-time control with sub-1 sec updates because of these issues.

Two demonstrations were conducted with the Prosperity and MdS hardware. The first ran the coordinated and uncoordinated controls with the same artificial PV power variability—established by disconnecting a portion of the PV array at specific times during the day. The results from this test indicated that the coordinated control would reduce the battery SOC range and extend the battery lifetime while still smoothing the PV power output. These results showed reasonable agreement with the simulations when the initial test conditions and communications were setup correctly; although, the magnitude of the benefits (SOC range reduction and battery energy throughput) were not as significant as in the simulations.

The 2<sup>nd</sup> demonstration was to compare coordinated and independent simulations to the results of the coordinated controller during a day with high PV variability. The results indicated that the battery throughput was reduced but the coordinated control actually utilized a greater portion of the battery SOC range. This effect was studied with a number of simulations and it was found that in cases of high variability the GE can remain above or below  $P_{GE\_nom}$  for long periods of time, thereby biasing  $P_{bat}$ , and resulting in a large SOC range with the coordinated controller. This was not seen in the previous simulations, but it is believed that incorporating a better return-to- $P_{GE\_nom}$  control mechanism (e.g. large  $K_{GE}$  gain), the SOC range with the coordinated control can be better maintained.

## REFERENCES

- [1] O. Lavrova, F. Cheng, S. Abdollahy, A. Mammoli, S. Willard, B. Arellano, and C. van Zeyl, "Modeling of PV plus Storage for Public Service Company of New Mexico's Prosperity Energy Storage Project," 2011 Electrical Energy Storage Applications & Technologies Conference (EESAT), San Diego, CA, Oct. 16-19, 2011.
- [2] A. Ellis and D. Schoenwald, PV Output Smoothing with Energy Storage, Sandia Technical Report, SAND2012-1772, March 2012.
- [3] A. Ellis and D. Schoenwald, "PV Output Smoothing with Energy Storage," Proceedings of the 38<sup>th</sup> IEEE Photovoltaic Specialists Conference, Austin, TX, 3-8 June 8, 2012.
- [4] S. Abdollahy, A. Mammoli, F. Cheng, A. Ellis, and J. Johnson, Distributed Compensation of a Large Intermittent Energy Resource in a Distribution Feeder, IEEE PES Innovative Smart Grid Technologies (ISGT), 24-27 Feb., 2013.
- [5] J. Johnson, A. Ellis, A. Denda, K. Morino, T. Shinji, T. Ogata, M. Tadokoro, "PV Output Smoothing using a Battery and Natural Gas Engine-Generator," 39th IEEE Photovoltaic Specialists Conference, Tampa Bay, Florida, 16-21 Jun, 2013.
- [6] T. Hund, S. Gonzalez, and K. Barrett, "Grid-Tied PV System Energy Smoothing," 35th IEEE Photovoltaic Specialists Conference (PVSC), Honolulu, HI, pp. 2762-2766, June 20-25, 2010.
- [7] H. Fakham, D. Lu, and B. Francois, "Power Control Design of a Battery Charger in a Hybrid Active PV Generator for Load-Following Applications," IEEE Transactions on Industrial Electronics, Vol. 58, No. 1, pp. 85-94, Jan. 2011.
- [8] M. Khalid, A.V. Savkin, A model predictive control approach to the problem of wind power smoothing with controlled battery storage, Renewable Energy, vol. 35, no. 7, pp. 1520-1526, July 2010.
- [9] S. Teleke, M.E. Baran, S. Bhattacharya, A.Q. Huang, "Optimal Control of Battery Energy Storage for Wind Farm Dispatching," *IEEE Transactions on Energy Conversion*, vol. 25, no. 3, pp. 787-794, Sept. 2010.
- [10] KEMA, Inc., Lanai PV Interconnect Requirements Study: System Impact Study, June 5, 2008, Interconnection Customer: SunPower, KEMA, Inc., Raleigh, NC, USA, 26707.
- [11] Puerto Rico Electric Power Authority, Minimum Technical Requirements for Interconnection of Photovoltaic Facilities, 2012.
- [12] M. Coddington and A. Ellis, Updating Interconnection Screens for PV Integration Can Streamline Deployment, Solar Industry, Vol. 5, No. 8. pp. 70-74, Sept. 2012.

- [13] P Denholm, E. Ela, B. Kirby, and M. Milligan, The Role of Energy Storage with Renewable Electricity Generation, NREL Technical Report, NREL/TP-6A2-47187, January 2010.
- [14] C. Lenox, PV and Energy Storage: Beyond the Hype, Solar Power International, 12 Sept. 2012.
- [15] OSIssoft, LLC, San Leandro, CA, URL: <http://www.osisoft.com/>, accessed 8 Jan, 2014.
- [16] P. Benvenuto, PI 101, Module 10: Compression Algorithm, OSIssoft Users Community, URL: <http://community.osisoft.com/index.php?/topic/1061-pi-101-module-10-compression-algorithm/>, accessed 8 Jan, 2014.

## DISTRIBUTION

1	MS1033	Jay Johnson	06112
1	MS1033	Abraham Ellis	06112
1	MS1033	Charles J. Hanley	06112
1	MS1108	Dan Borneo	06111
1	MS1108	Ross Guttromson	06113
1	MS1140	David A. Schoenwald	06113
1	MS0899	Technical Library	09532 ( <i>electronic copy</i> )



**Sandia National Laboratories**